

Article

Nanocrystalline Tin Oxide Nanofibers Deposited by a Novel Focused Electrospinning Method. Application to the Detection of TATP Precursors

José Pedro Santos ^{1,*}, María Jesús Fernández ¹, José Luis Fontecha ¹, Daniel Matatagui ^{1,2}, Isabel Sayago ¹, María Carmen Horrillo ¹ and Isabel Gracia ³

¹ GRIDSEN, Instituto de Tecnologías Físicas y de la Información (ITEFI-CSIC), Madrid 28006, Spain; E-Mails: mj.fernandez@csic.es (M.J.F.); joseluis.fontecha@csic.es (J.L.F.); daniel.matatagui@ccadet.unam.mx (D.M.); i.sayago@csic.es (I.S.); carmen.horrillo.guemes@csic.es (M.C.H.)

² Fotónica de Microondas, CCADET, Universidad Nacional Autónoma de México (UNAM), 04510 DF, Mexico

³ Instituto de Microelectrónica de Barcelona (IMB-CNM-CSIC), Barcelona 08193, Spain; E-Mail: isabel.gracia@imb-cnm.csic.es

* Author to whom correspondence should be addressed; E-Mail: jp.santos@csic.es; Tel.: +34-915-618-806; Fax: +34-914-117-651.

External Editor: W. Rudolf Seitz

Received: 21 October 2014; in revised form: 1 December 2014 / Accepted: 10 December 2014 / Published: 16 December 2014

Abstract: A new method of depositing tin dioxide nanofibers in order to develop chemical sensors is presented. It involves an electrospinning process with in-plane electrostatic focusing over micromechanized substrates. It is a fast and reproducible method. After an annealing process, which can be performed by the substrate heaters, it is observed that the fibers are intertwined forming porous networks that are randomly distributed on the substrate. The fiber diameters oscillate from 100 nm to 200 nm and fiber lengths reach several tens of microns. Each fiber has a polycrystalline structure with multiple nano-grains. The sensors have been tested for the detection of acetone and hydrogen peroxide (precursors of the explosive triacetone triperoxide, TATP) in air in the ppm range. High and fast responses to these gases have been obtained.

Keywords: electrospinning; tin oxide; nanofiber sensors; TATP detection

1. Introduction

One-dimensional nanostructured SnO₂ with a high surface to volume ratio has attracted special attention in the last years. These types of structures, with different morphologies such as SnO₂ nanowires, nanobelts, nanorods and nanofibers, are being fabricated via thermal oxidation, thermal evaporation, self-catalytic growth, molten salt synthesis and electrospinning [1–6]. Among the above-mentioned techniques, electrospinning has important advantages such as simplicity, low-cost, and easy mass production. It is one of the most useful methods for the fabrication of 1-D composite nanofibers by electrostatic stretching [6,7].

In the electrospinning process, fibers are usually produced by applying a high voltage to a viscous solution. Under the effect of a strong electric field, a solution drop formed at the end of a metal tip is highly electrified. It experiences two major types of electrostatic forces: a Coulombic force exerted by the external electric field and an electrostatic repulsion between surface charges [8]. With these electrostatic interactions, the droplet is distorted into a conical object (known as Taylor cone). As the voltage reaches a critical value, the electrostatic forces overcome the surface tension of the solution and an electrified jet is produced. The jet is subsequently stretched to form a continuous fiber.

Early works on electrospinning were realized with conventional organic polymers of high molecular weight [9], however as from the middle of this decade, great interest has emerged in the development of metal oxide fibers, such as CuO, SnO₂, TiO₂, ZnO, CeO₂, Ta₂O₅, through electrospinning of polymer solutions incorporating metal precursors and annealing processes [10–14]. In the electrospun process various reactions such as hydrolysis, condensation and gelation of the precursors are involved in the morphological and microstructural evolution of the fibers and after a final annealing process at elevated temperatures (≥ 300 °C), the organic components decompose and the inorganic precursors oxidize forming metal oxide nanofibers on the substrate. Due to their morphological properties, the nanofibers of metal oxides and the coupled oxide nanocomposites nanofibers are being used in gas sensor applications because they improve the gas-sensitive properties of the sensors [15–24]. It is well known that nanostructured shapes such as nanowires and nanofibers are very useful for fabricating gas sensors because of the high conductivity changes produced by the adsorption or desorption of very low concentrations of chemical species on the surface. Therefore in order to use them in gas sensors, it is necessary to identify the morphological parameters that define the surface of the nanofibers. It has been seen by microscopic techniques that individual electrospun nanofibers of oxide materials usually consist of nanosized grains and in addition, nanofiber networks are highly porous, which enhances the process of adsorption-desorption of gases [25,26]. The sensors are often coated with a thin layer of the sensitive material, in which the reaction with the volatiles takes place. In this case the sensitive area equals the active area of the device. The morphology of the sensing layer plays an important role in the molecular adsorption-desorption process, sensor response and sensitivity. In order to take advantage of the larger surface of reaction of the nanostructured materials, they can be used as sensitive layer instead of a thin layer, improving the sensitivity and velocity of the reaction. Therefore, sensitive

layers of nanostructured materials could provide better sensitivity than sensitive continuous thin films deposited by methods such as drop, airbrush or spinning.

In the present work, a new method of preparing SnO₂ nanofibers synthesized by electrospinning is proposed. It involves a focused electrospinning system and annealing process after electrospinning a PVA/SnCl₄·5H₂O composite. Scanning electron microscopy (SEM) and X-ray diffractometry (XRD) were used for characterizing the nanofibers. The sensors have been tested for the detection of low concentrations of acetone and hydrogen peroxide, precursors of triacetone triperoxide (TATP) used in improvised explosive devices (IEDs) [27].

2. Materials and Methods

2.1. Electrospinning Precursor

An electrospinning method was used to synthesize SnO₂ nanofibers. The electrospun solution was prepared from a PVA/SnCl₄·5H₂O composite. First, a solution of poly(vinyl alcohol) (PVA) with molecular weight of Mw ~170,000 (Sigma-Aldrich, St. Louis, MO, USA) was prepared by dissolving the PVA powder (8%) in deionized water and stirring at 90 °C during 4 h. A solution of tin (IV) chloride pentahydrate (SnCl₄·5H₂O, Sigma-Aldrich, 2 g) in deionized H₂O (2 g) was prepared at room temperature as the precursor material. This solution was slowly added into the PVA solution (20 g) and stirred at room temperature for 2 h. The inorganic/organic composite solution prepared was loaded into syringe with a stainless steel needle whose external diameter was 0.6 mm.

2.2. Electrospinning Setup and Electrospinning Process (ESEP)

In the electrospinning process, the solution in the syringe is extruded from the needle tip to the collector, where the device is placed. When high voltage is applied between the needle and the collector, an electrostatic force is induced on the droplets of the solution that are in the needle tip. The interaction between this electrostatic force and surface tension causes the droplets to stretch, forming thin jets of polymer solution which dry in flight and then are deposited onto the collector.

In the usual electrospinning setup, the needle is connected to a high-voltage power supply and directed to the grounded collector, a conductor plate, obtaining random fibers, because of the wide distribution of the electric field generated by the needle and the collector when a high voltage is applied between them (Figure 1a). Therefore, it is difficult to electrospin fibers in specific positions. Taking into account that our target area is small (the whole sensor has a diameter of about 10 mm), it is essential to reduce the area of deposition of the nanofibers in order to avoid that they could be torn when the sensor is handled after the nanofiber deposition. Usually the focusing is achieved with electrostatic lens systems, which have ring electrodes between the needle and the substrate [28]. We propose a new simpler method: in plane focusing.

A study of the electric field distribution has been carried out for reducing the fibers deposition area modifying the electrode and collector shape and reducing the needle to collector distance. To perform the required simulations of the modified deposition system, the simulation software Comsol was used. The study took account of the shapes of electrodes, the distance between them and the voltages applied to all them. Figure 1b shows the configuration of the electric field lines when the components are

placed in the optimal position and they are fed with the optimal values of the voltages, which finally were used in this work. It can be seen that the electric field lines are concentrated towards the sensor. In fact, we can say that, with this configuration, no fibers were deposited outside the sensor area. A photograph of the nanofiber deposition zone of this structure is presented in Figure 2a. On the left the needle protruding the square metallic screen can be seen and at the right part, the collector structure, consisting of a square metal plate with a central circular window in whose center the sensor is located.

The setup for electrospinning consisted of a 10 mL glass syringe in which a 1 m length microtube was connected in the outlet, which linked the syringe with a metallic needle of 0.6 mm of external diameter. This needle was modified by removing the beveled portion of the tip to let the final cut be perpendicular to its axis. The syringe, was placed in the syringe pump (KD Scientific 210, Holliston, MA, USA) where the solution flow rate was selected, which in this work was optimized to $5 \mu\text{L}\cdot\text{min}^{-1}$. The needle is inserted on a flat 100 mm side square conductor, both fed with a voltage of 18 kV. The collector structure is divided into two parts, an inner circle of diameter 15 mm where the sensor is centered and a 200 mm side metal square whose inner limit is a circle of 60 mm diameter concentric to the circle where the target is placed. The target is set to 0 V and the outer metallic plate is set to 1 kV. The tip of the needle protrudes 15 mm from the square screen and the distance from the needle tip to the sensor is 40 mm. Electrospinning time varied from 60 to 180 s. Figure 2b shows the schematic diagram of the experimental setup.

Nanofibers were electrospun onto two different micromechanized substrates. The first one is a single microhotplate with interdigitated electrodes in a TO-5 package (Cambridge CCS503_17A, Cambridge, UK). The second one is a four microhotplates device in a TO-8 package developed at CNM [29]. Individual sensors could be heated up to $550 \text{ }^\circ\text{C}$ with power consumption in the order of tens of mW. All substrates with electrospun fibers were annealed between $450 \text{ }^\circ\text{C}$ and $550 \text{ }^\circ\text{C}$ in ambient atmosphere for 4 hours using a tube furnace with a temperature ramp of $4 \text{ }^\circ\text{C}/\text{min}$.

Figure 1. Simulation, using the software Comsol, of the equipotential lines and the direction and intensity of the electric field in the structures described above. (a) Usual electrospinning; (b) Focused setup used in this work.

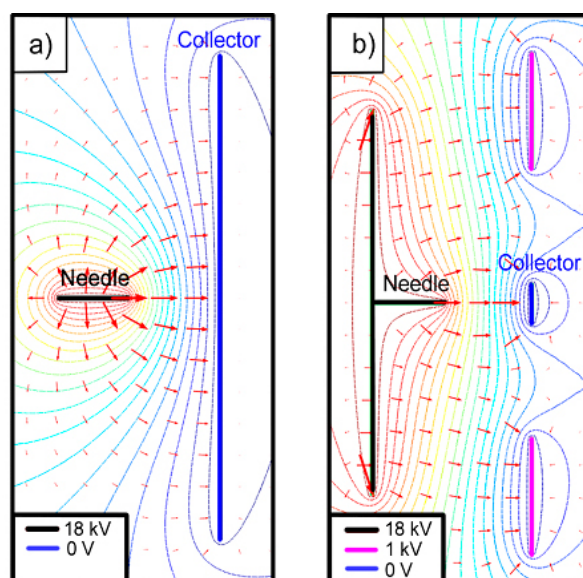
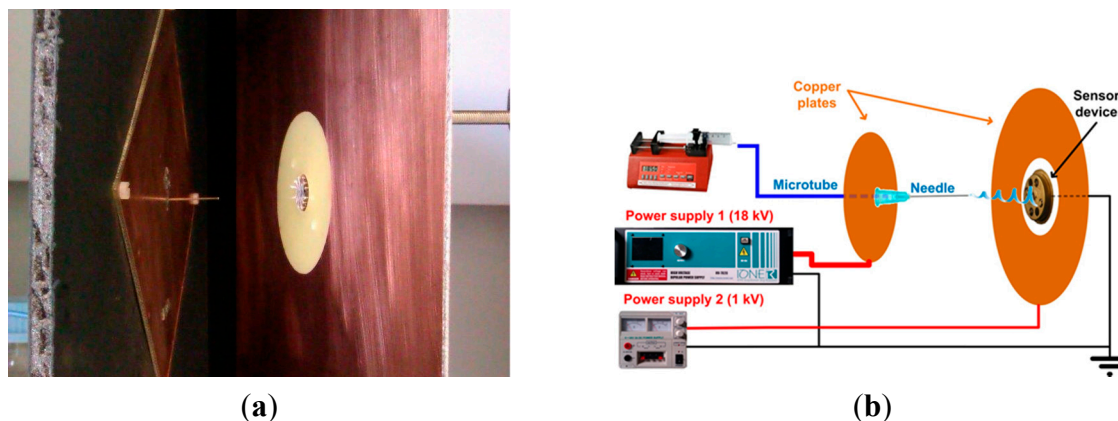


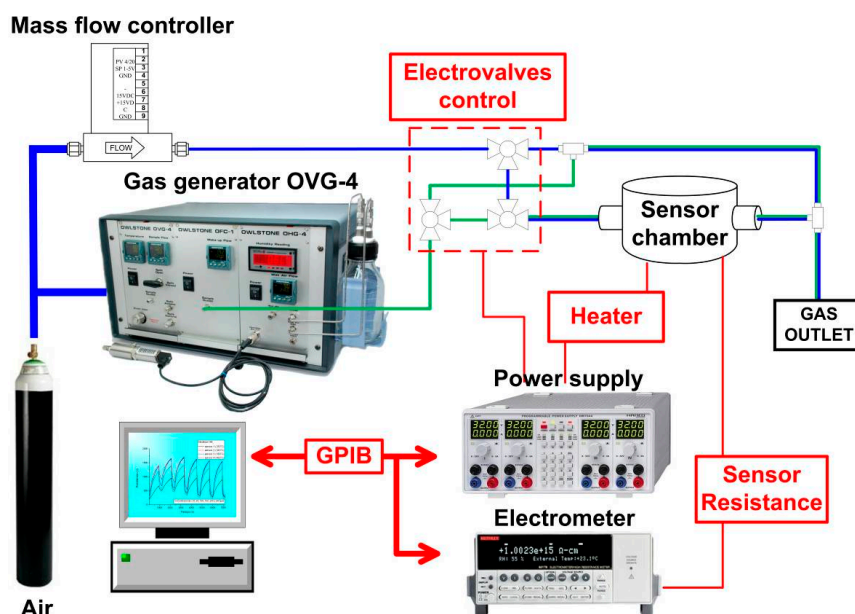
Figure 2. (a) Image of the electrodes in the nanofibers deposition: to the left, the source with the needle and the metal screen, both at 18 kV, and in the right part, the focus metal square plate at 1 kV, and the target in its center at 0 V; (b) Schematic illustration of the electrospinning setup.



2.3. Gas Line Setup

A scheme of the gas measurement setup is shown in Figure 3. The vapors were generated by a OVG-4 vapour generator (Owlstone, Cambridge, UK) through calibrated permeation tubes. Sensor resistance was measured by an electrometer with a scanner card (6517 and 6522, Keithley, Cleveland, OH, USA). Voltage for the sensor heaters was provided by a programmable power supply (HM7044, Hameg, Mainhausen, Germany). Both instruments were controlled by a PC through a GPIB interface. Measurements were made at a constant flow of 50 mL/min. Adsorption time was 5 min and desorption times varied between 60 min and 120 min. At least five measurements were made for each concentration and the mean and standard deviation were recorded.

Figure 3. Measurement setup.

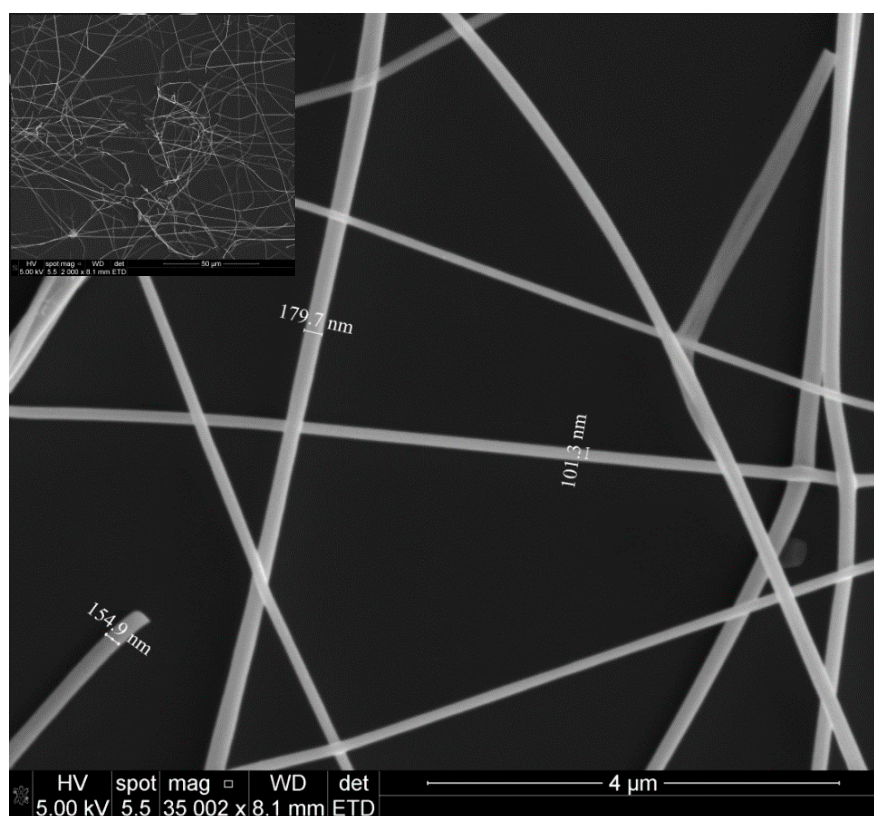


3. Results and Discussion

3.1. Morphological Characterization

The microstructure of the fibers was investigated by SEM (Quanta 3d FEG, FEI, Hillsboro, OR, USA) and XRD (D8 Advance, Bruker, Fremont, CA, USA). The SEM images of SnO₂ nanofibers annealed at 450 °C for 4 h in air are shown in Figure 4. The fibers were intertwined forming porous networks that are randomly distributed on the substrate, as can be seen in Figure 5. In general, the fiber diameters oscillated from 100 nm to 200 nm and fiber lengths reached several tens of microns. It is interesting to note that each fiber had a polycrystalline structure with multiple nanograins as shown in the SEM image of Figure 5 and confirmed by XRD analysis.

Figure 4. SEM images of SnO₂ nanofibers annealed at 450 °C for 4 h in air. The inset figure is a low-magnification image, showing the overall feature of the electrospun fibers.



The dimensions of these grains increased with annealing temperature and varied from a few nanometers for those annealed at 450 °C (Figure 5a) to tens of nanometers for those annealed at 550 °C (Figure 5b). In next subsection we will see that it will have a great impact in gas sensing properties.

The Energy Dispersive Spectroscopy (EDS) analysis (Figure 6) confirmed that the samples (nanofibers) contain O and Sn atoms. The Si signal was due to the substrate. The X-ray diffractograms show that the fibers are composed by tin dioxide (cassiterite) with preferential orientations (111), (211) and (310). From the broadening of the peaks we can estimate the grain sizes applying Scherrer's equation. Results obtained are in good agreement with the values calculated from the SEM images.

The characteristics of the fibers (with multiple nanograins) and porosity of the obtained samples are features particularly useful for gas sensing applications where the surface plays an important role in the detection process [30,31].

Figure 5. Detail of nanofibers showing their nanostructure. (a) Grain sizes of few nanometers after annealing at 450 °C; (b) grain sizes of tens of nanometers after annealing at 550 °C.

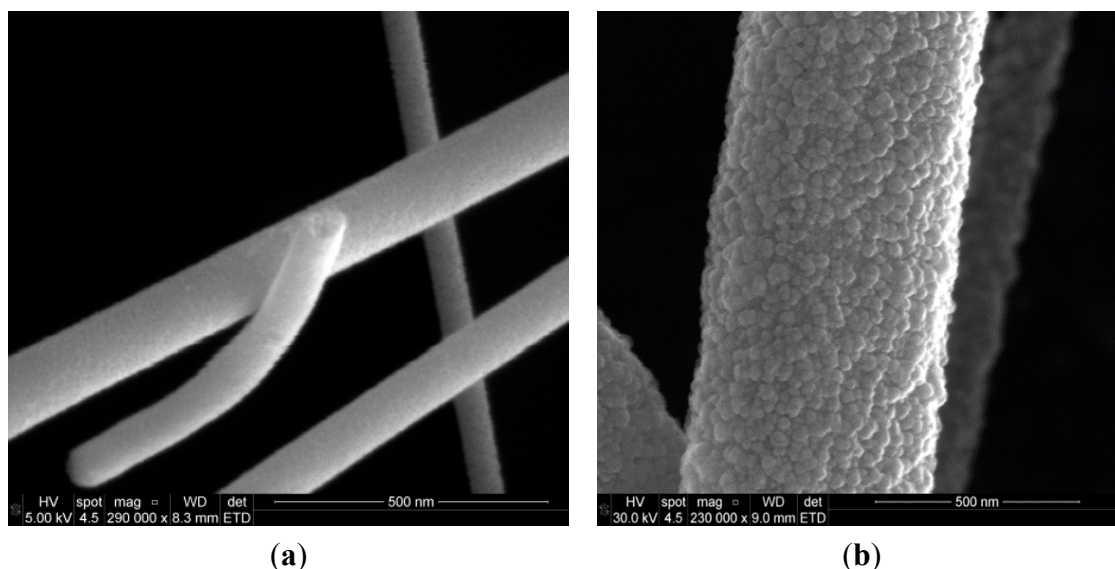
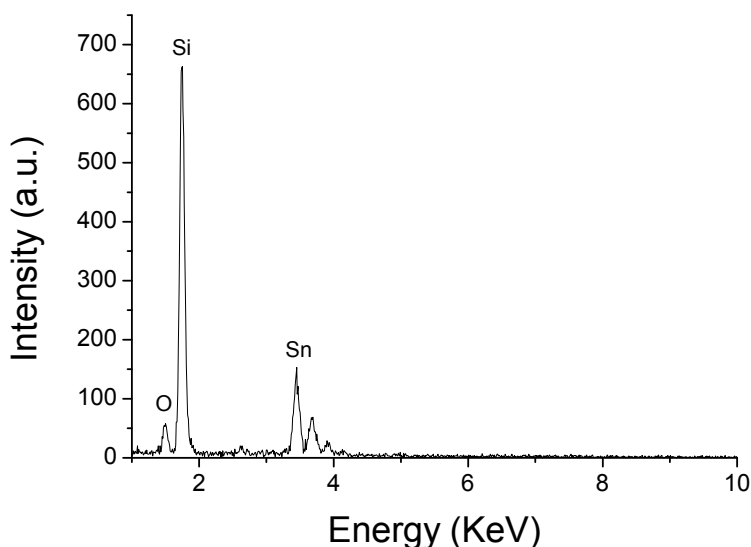


Figure 6. EDX spectrogram of the SnO₂ nanofiber sensor.

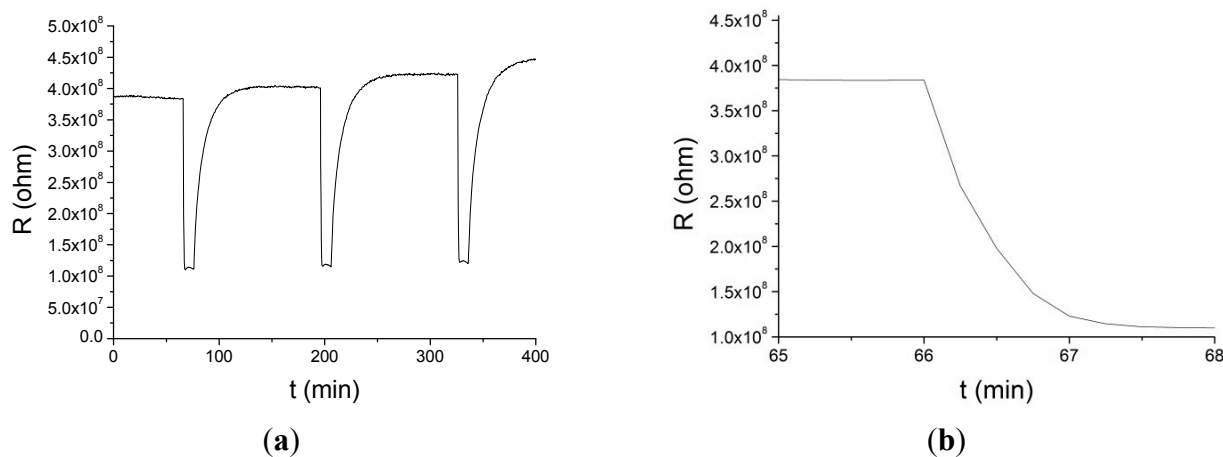


3.2. Gas Sensing Properties

These nanofiber-based sensors have been tested in air with acetone at concentrations varying from 2 ppm to 70 ppm and hydrogen peroxide in concentrations from 5 ppm to 180 ppm. The maximum response was obtained around 350 °C–400 °C and with short electrospinning times. In Figure 7a the resistance change of a nanofiber sensor to 5 ppm of acetone at 400 °C is shown.

Figure 7b shows a detail of Figure 7a around the first adsorption cycle that shows the fast response time of the sensor.

Figure 7. (a) Response of a nanofiber sensor with 90 s deposition time and 450 °C annealing temperature to 5 ppm of acetone at 400 °C; (b) expanded area around the first adsorption cycle.



Sensor temperatures varied from 200 to 400 °C. Resistance of the sensors was in the range from $10^6 \Omega$ to $10^{10} \Omega$. Response times were of the order of few seconds (15 s for 2 ppm of acetone at 350 °C) decreasing with operation temperature increase for both compounds. These times are of the same order or lower than those reported for other acetone nanofiber or thin film sensors [32,33].

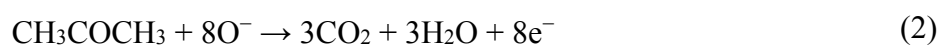
We have not found any literature reporting hydrogen peroxide nanofiber sensors. The curves are repetitive, although a slight drift is observed. Sensor response for acetone is defined as follows:

$$r (\%) = 100 \times (R_a / R_s) \quad (1)$$

where R_a is the resistance in air and R_s is the minimum resistance of the sensor exposed to the sample. For hydrogen peroxide the definition is the inverse of Equation (1) because of its oxidizing nature. In the response curves the mean and standard deviations of this value are represented.

Figure 8 shows the response to the whole acetone range at 350 °C and 400 °C. Figure 9 shows the response to hydrogen peroxide at 300 °C and 400 °C. In this case the response changes with temperature were less remarkable than with acetone. It must be noted that sensors annealed at 450 °C had higher responses than sensors annealed at higher temperatures. In fact sensors annealed at 450 °C had a maximum response higher than 400% to 70 ppm of acetone, whereas sensors annealed at 550 °C did not reach 100% for the same concentration.

For acetone the response mechanism is based on the reaction of the acetone molecule with the adsorbed oxygen:



with the releasing of the trapped electrons to the conduction band and decreasing of the resistance [34].

Figure 8. Response of a nanofiber sensor with 120 s deposition time and 450 °C annealing temperature to acetone at 350 °C and 400 °C.

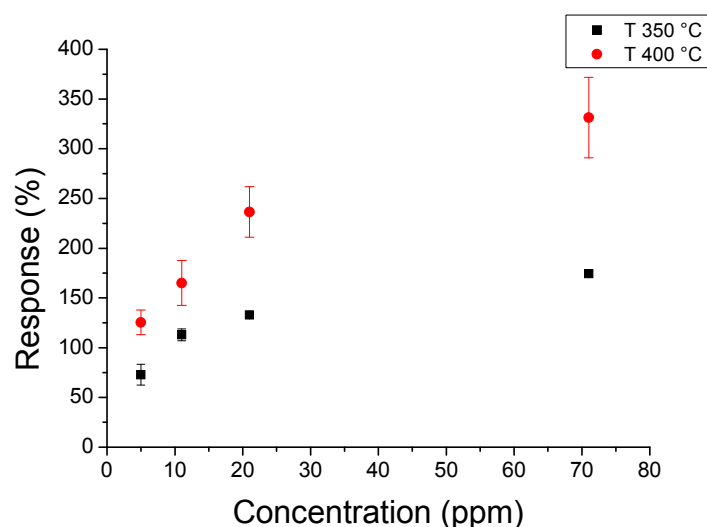
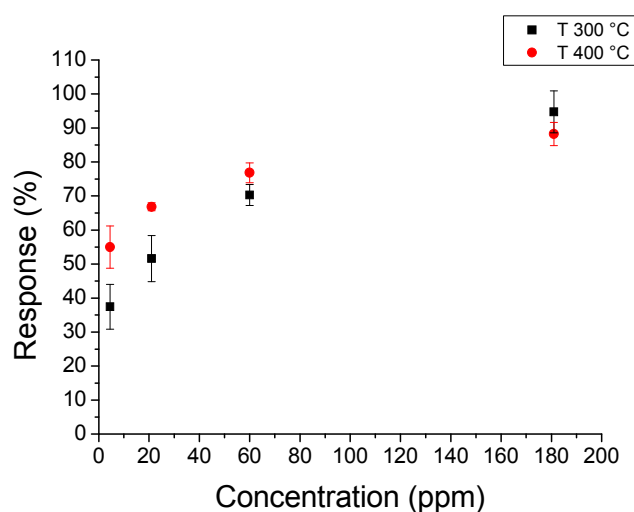


Figure 9. Response of a nanofiber sensor with 180 s deposition time and 450 °C annealing temperature to hydrogen peroxide at 300 °C and 400 °C.



In the case of the hydrogen peroxide the mechanism is the following [35]:

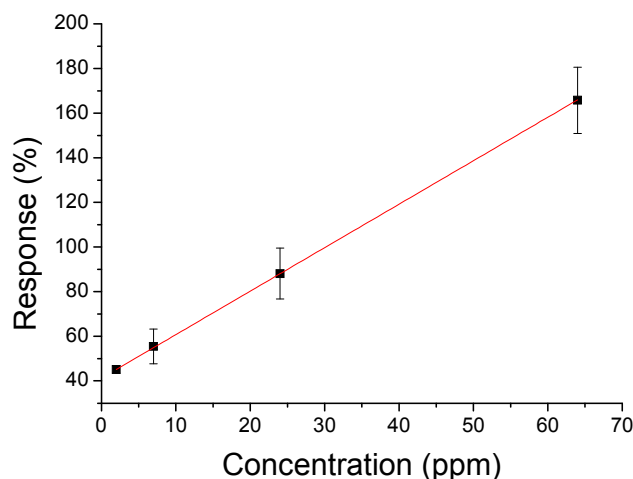


where M is a surface adsorption site. The result is the trapping of conduction electrons and thus increasing the resistance.

Response times of the order of few seconds are an improvement over thin film sensors that have response times of the order of minutes [35–37]. This is mainly due to the porous structure of the sensors which allows quick gas diffusion, as can be seen from the SEM images. Differences in responses can be attributed to different grain sizes, a well-known effect in nanocrystalline tin dioxide [38–40]. Sensors annealed at 450 °C have smaller grain sizes than sensors annealed at 550 °C,

thus the responses of the former are greater than the response of the latter. Although the majority of the responses obeyed to a power law we found a few sensors with linear behavior (Figure 10).

Figure 10. Linear response of a sensor with 90 s deposition time and 450 °C annealing temperature to acetone at 300 °C.



The difference in response curve shapes has been explained in the framework of the electron theory of adsorption where the main parameter is the density of chemisorbed sites at the surface [38]. According to this theory surface oxygen vacancies act as chemisorption sites and small variations from the theoretical value from bulk value lead to different response curve shapes. It has been shown that the tin oxide surface is quite complex and variable oxygen composition of oxide surfaces has been reported [41]. In our case, at same annealing temperature, the only deposition parameter that changes is electrospinning time although it is not clear the way it affects the density of surface adsorption sites and it deserves further research.

4. Conclusions

The electrospinning technique is an efficient method for depositing tin oxide nanofibers. We have developed a novel focusing scheme to deposit the fibers onto small areas. The nanofibers were used as sensitive layers for resistive chemical sensors showing high sensitivity, high reproducibility and fast response time in the detection of TATP explosive precursors in the ppm range. The sensors exhibited high and fast responses in a wide operating temperature range. Maximum response values have been obtained with short deposition times at 450 °C annealing temperature. Sensing characteristics as response value and response curve shape were dependent on preparation parameters such as deposition time and annealing temperature.

Acknowledgments

This work has been supported by the Spanish Science and Innovation Ministry under the projects TEC2010-21357-C05-04 and TEC2013-48147-C6-4-R. Authors want to thank University of Extremadura for SEM and XRD analysis.

Author Contributions

This work was a result of the collaboration among the authors. José Pedro Santos directed the research and performed the data acquisition. María Jesús Fernández prepared the precursors and performed the electrospinning. José Luis Fontecha designed the experimental electrospinning setup. Daniel Matatagui made the Comsol simulations. Isabel Gràcia fabricated the chip. Isabel Sayago performed the fiber characterization. Maria Carmen Horrillo corrected the final version of the manuscript. All authors discussed, edited and approved the final version of the paper.

Conflicts of Interest

The authors declare no conflict of interest.

References

1. Wang, D.; Chu, X.F.; Gong, M.L. Gas-sensing properties of sensors based on single-crystalline SnO₂ nanorods prepared by a simple molten-salt method. *Sens. Actuators B Chem.* **2006**, *117*, 183–187.
2. Yang, M.R.; Chu, S.Y.; Chang, R.C. Synthesis and study of the SnO₂ nanowires growth. *Sens. Actuators B Chem.* **2007**, *122*, 269–273.
3. Luo, S.H.; Fan, J.Y.; Liu, W.L.; Zhang, M.; Song, Z.T.; Lin, C.L.; Wu, X.L.; Chu, P.K. Synthesis and low-temperature photoluminescence properties of SnO₂ nanowires and nanobelts. *Nanotechnology* **2006**, *17*, 1695–1699.
4. Comini, E.; Faglia, G.; Sberveglieri, G.; Calestani, D.; Zanotti, L.; Zha, M. Tin oxide nanobelts electrical and sensing properties. *Sens. Actuators B Chem.* **2005**, *111–112*, 2–6.
5. Hu, J.Q.; Bando, Y.; Golberg, D. Self-catalyst growth and optical properties of novel SnO₂ fishbone-like nanoribbons. *Chem. Phys. Lett.* **2003**, *372*, 758–762.
6. Dharmaraj, N.; Kim, C.H.; Kim, K.W.; Kim, H.Y.; Suh, E.K. Spectral studies of SnO₂ nanofibers prepared by electrospinning method. *Spectrochim. Acta A* **2006**, *64*, 136–140.
7. Yu-Jin, L.; Hyo-Jin, A. Fabrication of uniform SnO₂-SiO₂-Pt composite nanofibres via co-electrospinning. *Ceram. Int.* **2013**, *39*, 5303–5038.
8. Li, D.; Xia, Y.N. Electrospinning of nanofibers: Reinventing the wheel? *Adv. Mater.* **2004**, *16*, 1151–1170.
9. Huang, Z.M.; Zhang, Y.Z.; Kotaki, M.; Ramakrishna, S. A review on polymer nanofibers by electrospinning and their applications in nanocomposites. *Compos. Sci. Technol.* **2003**, *63*, 2223–2253.
10. Guan, H.; Shao, C.; Chen, B.; Gong, J.; Yang, X. A novel method for making CuO superfine fibers via an electrospinning technique. *Inorg. Chem. Commun.* **2003**, *6*, 1409–1411.
11. Macias, M.; Chacko, A.; Ferraris, J.P.; Balkus, K.J. Electrospun mesoporous metal oxide fibers. *Micropor. Mesopor. Mater.* **2005**, *86*, 1–13.
12. Yang, X.H.; Shao, C.L.; Guan, H.Y.; Li, X.L.; Gong, J. Preparation and characterization of ZnO nanofibers by using electrospun PVA/zinc acetate composite fiber as precursor. *Inorg. Chem. Commun.* **2004**, *7*, 176–178.

13. Onozuka, K.; Ding, B.; Tsuge, Y.; Naka, T.; Yamazaki, M.; Sugi, S.; Ohno, S.; Yoshikawa, M.; Shiratori, S. Electrospinning processed nanofibrous TiO₂ membranes for photovoltaic applications. *Nanotechnology* **2006**, *17*, 1026–1031.
14. Yang, X.H.; Shao, C.L.; Liu, Y.C.; Mu, R.X.; Guan, H.Y. Nanofibers of CeO₂ via an electrospinning technique. *Thin Solid Films* **2005**, *478*, 228–231.
15. Ding, B.; Wang, M.; Yu, J.; Sun, G. Gas Sensors Based on Electrospun Nanofibers. *Sensors* **2009**, *9*, 1609–1624.
16. Ding, B.; Kim, J.; Miyazaki, Y.; Shiratori, S. Electrospun nanofibrous membrane coated quartz crystal microbalance as gas sensor for NH₃ detection. *Sens. Actuators B Chem.* **2004**, *101*, 373–380.
17. Liu, H.Q.; Kameoka, J.; Czaplewski, D.A.; Craighead, H.G. Polymeric nanowire chemical sensor. *Nano Lett.* **2004**, *4*, 671–675.
18. Kessick, R.; Tepper, G. Electrospun polymer composite fiber arrays for the detection and identification of volatile organic compounds. *Sens. Actuators B Chem.* **2006**, *117*, 205–210.
19. Luoh, R.; Hahn, H.T. Electrospun nanocomposite fiber mats as gas sensors *Compos. Sci. Technol.* **2006**, *66*, 2436–2441.
20. Kim, I.D.; Rothschild, A.; Lee, B.H.; Kim, D.Y.; Jo, S.M.; Tuller, H.L. Ultrasensitive chemiresistors based on electrospun TiO₂ nanofibers. *Nano Lett.* **2006**, *6*, 2009–2013.
21. Zhang, Y.; He, X.L.; Li, J.P.; Miao, Z.J.; Huang, F. Fabrication and ethanol-sensing properties of micro gas sensor based on electrospun SnO₂ nanofibers. *Sens. Actuators B Chem.* **2008**, *132*, 67–73.
22. Wang, G.; Ji, Y.; Huang, X.R.; Yang, X.Q.; Gouma, P.I.; Dudley, M. Fabrication and characterization of polycrystalline WO₃ nanofibers and their application for ammonia sensing. *J. Phys. Chem. B* **2006**, *110*, 23777–23782.
23. Khorami, H.A.; Keyanpour-Rad, M.; Reza Vaezi, M. Synthesis of SnO₂/ZnO composite nanofibers by electrospinning method and study of its ethanol sensing properties. *Appl. Surf. Sci.* **2011**, *257*, 7988–7992.
24. Zhao, Y.; He, X.; Li, J.; Cao, X.; Jia, J. Porous CuO/SnO₂ composite nanofibers fabricated by electrospinning and their H₂S sensing properties. *Sens. Actuators B Chem.* **2012**, *165*, 82–87.
25. Park, J.Y.; Asokan, K.; Choi, S.W.; Kim, S. Growth kinetics of nanograins in SnO₂ fibers and size dependent sensing properties. *Sens. Actuators B Chem.* **2011**, *152*, 254–260.
26. Zhang, Y.; Li, J.; An, G.; He, X. Highly porous SnO₂ fibers by electrospinning and oxygen plasma etching and its ethanol-sensing properties. *Sens. Actuators B Chem.* **2010**, *144*, 43–48.
27. Önerud, H.; Wallin, S.; Östmark, H.; Menning, D.; Ek, S.; Ellis, H.; Kölhed, M. Localisation of threat substances in urban society-LOTUS: A viable tool for finding illegal bomb factories in cities. In *Sensors, and Command, Control, Communications, and Intelligence (C3I) Technologies for Homeland Security and Homeland Defense X*; SPIE: Bellingham, WA, USA; 2011.
28. Neubert, S.; Pliszka, D.; Góra, A.; Jaworek, A.; Wintermantel, E.; Ramakrishna, S. Focused deposition of electrospun polymer fibers. *J. Appl. Polym. Sci.* **2011**, *125*, 820–827.
29. Horrillo, M.C.; Martí, J.; Matatagui, D.; Santos, J.P.; Sayago, I.; Gutiérrez, J.; Martín-Fernández, I.; Ivanov, P.; Gràcia, I.; Cané, C. Single-walled carbon nanotube microsensors for nerve agent simulatant detection. *Sens. Actuators B Chem.* **2011**, *157*, 1253–1259.

30. Rickerby, D.G.; Horrillo, M.C.; Santos, J.P.; Serrini, P. Microstructural characterization of nanograin tin oxide gas sensors. *Nanostr. Mat.* **1997**, *9*, 43–52.
31. Agapito, J.A.; Santos, J.P. The interaction of low NO₂ concentrations in air with degenerate nanocrystalline tin dioxide thin films. *Sens. Actuators B Chem.* **1996**, *31*, 93–98.
32. Cheng, L.; Ma, S.Y.; Li, X.B.; Luo, J.; Li, W.Q.; Li, F.M.; Mao, Y.Z.; Wang, T.T.; Li, Y.F. Highly sensitive acetone sensors based on Y-doped SnO₂ prismatic hollow nanofibers synthesized by electrospinning. *Sens. Actuators B Chem.* **2014**, *200*, 181–190.
33. Choi, J.; Lee, J.; Choi, J.; Jung, D.; Shim, S.E. Electrospun PEDOT: PSS/PVP nanofibers as the chemiresistor in chemical vapour sensing. *Synth. Met.* **2010**, *160*, 1415–1421.
34. Qin, L.; Xu, J.; Dong, X.; Pan, Q.; Cheng, Z.; Xiang, Q.; Li, F. The template-free synthesis of square-shaped SnO₂ nanowires: the temperature effect and acetone gas sensors. *Nanotechnology* **2008**, *19*, 185705–185712.
35. Hiroki, A.; La Verne, J.A. Decomposition of Hydrogen Peroxide at Water-Ceramic Oxide Interfaces. *J. Phys. Chem. B* **2005**, *109*, 3364–3370.
36. Rella, R.; Spadavecchia, J.; Manera, M.G.; Capone, S.; Taurino, A.; Martino, M.; Caricato, A.P.; Tunno, T. Acetone and ethanol solid-state gas sensors based on TiO₂ nanoparticles thin film deposited by matrix assisted pulsed laser evaporation. *Sens. Actuators B Chem.* **2007**, *127*, 426–431.
37. Patil, S.B.; Patil, P.P.; More, M.A. Acetone vapour sensing characteristics of cobalt-doped SnO₂ thin films. *Sens. Actuators B Chem.* **2007**, *125*, 126–130.
38. Santos, J.P.; Agapito, J.A. The interaction of oxygen with nanocrystalline SnO₂ thin films in the framework of the electron theory of adsorption. *Thin Solid Films* **1999**, *338*, 276–280.
39. Panchapakesan, B.; Cavicchi, R.; Semancik, S.; De Voe, D.L. Sensitivity, selectivity and stability of tin oxide nanostructures on large area arrays of microhotplates. *Nanotechnology* **2006**, *17*, 415–425.
40. Rothschild, A.; Komem, Y. The effect of grain size on the sensitivity of nanocrystalline metal-oxide gas sensors. *J. Appl. Phys.* **2004**, *95*, 6374–6380.
41. Batzill, M. Surface Science Studies of Gas Sensing Materials: SnO₂. *Sensors* **2006**, *6*, 1345–1366.

© 2014 by the authors; licensee MDPI, Basel, Switzerland. This article is an open access article distributed under the terms and conditions of the Creative Commons Attribution license (<http://creativecommons.org/licenses/by/4.0/>).